Characterization Methods for the State of Charge Estimation of Lithium-ion Batteries

F. Conte, S. Massucco, M. Saviozzi, F. Silvestro
DITEN, Università degli Studi di Genova,
via all'Opera Pia, 11/A I-16145, Genova, Italy
Email: stefano.massucco@unige.it

S. Grillo
DEIB, Politecnico di Milano,
p.zza Leonardo da Vinci, 32, I-20133, Milano, Italy
Email: samuele.grillo@polimi.it

***Abstract*—State of charge (SOC) estimation is an important task when managing batteries. This estimation, in fact, influences the control policies of these devices, especially when optimization algorithms are used to determine the set points of the power requested from (supplied to) them. The reliability of this estimation is affected by the accuracy with which the parameters of the dynamical model of the battery have been derived. This paper compares the effects of parameters identification on state of charge estimation algorithm. The comparison are performed on a real Lithium-Ion cell, whose parameters are identified using electrochemical impedance spectroscopy and autoregressive-moving-average model with exogenous inputs. Thus, the two models are used for state of charge estimation by means of a Kalman-filter-based algorithm. Three charge/discharge profiles are repeated in order to test the cell at different starting SOCs. The experimental results confirm that different methods for parameters identification lead to different (possibly inaccurate) SOCs.**

I. Introduction

Energy storage devices are gaining importance in the management of power systems, distribution grids, and microgrids [1], [2], [3], [4]. There are several challenges concerning energy storage devices' modeling and management (e.g., the identification of accurate models for predicting batteries ageing [5] and for an efficient exploitation of batteries' capabilities according to the particular operating conditions [6]). A reliable identification of the parameters of a battery model is crucial for all those algorithms that rely on accurate estimation of the state of the device, being the state of charge (SOC) the most important variable to be monitored [7], [8].

SOC estimation has been studied in many papers and different techniques have been proposed to tackle this problem (some more promising than others). In [9] a PI-based observer is proposed. The key feature of this technique is the ability to dynamically update the values of the equivalent circuit parameters, especially the equivalent capacitance of the battery. In [10], a review of the main techniques used for SOC estimation is presented and results obtained by using Kalman filter technique are compared with those obtained by means of Ampere-hour-counting (also known as Coulomb-counting). Authors state that electrochemical impedance spectroscopy (EIS) technique had not been effectively applied to SOC estimation problems till then.

In [11], EIS technique, combined with extended Kalman filter (EKF), is used, but the focus of the work is more on the impedance estimation, rather than on evaluating the effects that this estimation has on SOC. In [12], both EIS and EKF are used for effective SOC estimation. However, the comparison is performed with the Coulomb-counting technique, which may not be reliable, especially in case of measurement errors [9], [13].

In [14], authors propose an EKF-based estimator. In this paper the SOC is one of the estimated variables and the open-circuit voltage (OCV) of the cell is derived using a detailed electrical equivalent model of the cell itself, taking into account also hysteresis effects. The approach proposed in the present work is similar, but uses a less complex equivalent model, thus allowing an easier parameter identification process, and estimates the SOC by inverting the measured SOC-OCV map, rather than directly estimating the SOC and then calculating the OCV.

The main contribution of the present paper is the quantitative comparison of the results obtained using two different methodologies for identifying the parameters of a battery equivalent model. In particular, the two approaches are based on EIS and autoregressive-moving-average model with exogenous inputs (ARMAX) techniques. The former derives the values of the model parameters by means of a spectral analysis, while the latter exploits the time-domain characteristics of controlled charge and discharge tests.

The comparison, rather than being based on the numerical outputs of these two methodologies, is performed by looking at the results obtained by a Kalman-filter-based SOC estimation algorithm. The whole procedure has been validated on a Lithium-Ion cell tested using three different drive cycles. This resulted in an extensive comparison of the results of a Kalman-based on-line SOC estimation using real-life current profiles at different starting SOC levels. This comparison (based on real SOC values inferred from measured OCVs after adequate rest-time periods, as described in Section IV) demonstrates how a more comprehensive identification of the battery model parameters helps in obtaining a more effective SOC estimation. This methodology for the evaluation of the estimation error is not conventional, but assures a more accurate validation.

The paper is organized as follows. Section II describes the two characterization methods (i.e., EIS and ARMAX) of a Lithium-Ion battery cell. In this Section, the numerical results of the two methods are also reported. Section III describes a proper SOC estimation method for analyzing the impact of the two characterization methods on the estimation accuracy. In Section IV the evaluation results are presented. Finally, conclusions are drawn in Section V.

II. Characterization Methods

A. Model Description

The Lithium-Ion battery has been modeled as a second order equivalent electrical circuit [8], [15], [16], [17]. The circuit scheme is depicted in Figure 1.

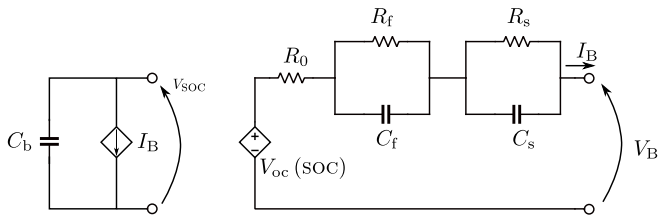

Figure 1. Two RC parallel branches equivalent circuit of the cell.

The battery SOC [%] is given by the voltage V_SOC across the whole-charge capacitor C_b through the relation: $\mathrm{SOC} = V_\mathrm{SOC}/V^\mathrm{nom} \times 100$, where V^nom is the battery rated voltage. The model defines the dynamical relation between SOC and the measured terminal voltage V_B and load current I_B. Accordingly to Figure 1, V_B can be defined as:

$$V_\mathrm{B} = V_\mathrm{oc}\,(\mathrm{SOC}) - V_\mathrm{f} - V_\mathrm{s} - R_0 I_\mathrm{B}, \tag{1}$$

where:

- $V_\mathrm{oc}(\mathrm{SOC})$ is the nonlinear mapping from the battery SOC and the open-circuit voltage V_oc [V];
- V_f and V_s [V] are the voltages of the two RC networks $(R_\mathrm{f}, C_\mathrm{f})$ and $(R_\mathrm{s}, C_\mathrm{s})$, respectively;
- R_0 [Ω] is the internal battery resistance.

The dynamics of V_f, V_s and V_SOC are given by:

$$\dot{V}_\mathrm{f} = -\frac{1}{R_\mathrm{f} C_\mathrm{f}} V_\mathrm{f} + \frac{1}{C_\mathrm{f}} I_\mathrm{B} \tag{2}$$

$$\dot{V}_\mathrm{s} = -\frac{1}{R_\mathrm{s} C_\mathrm{s}} V_\mathrm{s} + \frac{1}{C_\mathrm{s}} I_\mathrm{B} \tag{3}$$

$$\dot{V}_\mathrm{SOC} = -\frac{1}{C_\mathrm{b}} I_\mathrm{B} \tag{4}$$

B. Electrochemical Impedance Spectroscopy Procedure

Electrochemical impedance spectroscopy (EIS) [18] is a methodology for the characterization of electrochemical equipment. The basic principle is to perturb the steady-state operating point by injecting a small-signal ac current, measure the voltage, and derive the complex impedance $Z\,(j\omega)$ from the ratio between voltage and current phasors. By spanning an appropriately wide range of frequencies the characteristic Nyquist plots can be drawn. As this methodology is usually performed for capacitive elements, these graphs are built by plotting the results on the complex plane $(\Re, -\Im)$. Information contained in such graphs are extremely useful because they give the indication on how the impedance changes (not only numerically, i.e., in its absolute value, but also in its dynamical behavior, i.e., in the way the real and imaginary parts of the impedance reciprocally vary).

Data obtained through EIS, in particular, can be used to fit the parameters of a model (such as the one in Figure 1). The fitting can be performed by minimizing the normalized mean squared error. Let N be the number of injected frequencies, $\boldsymbol{e}$ be the column vector of the errors between the equivalent impedance model $\boldsymbol{Z}\,(\omega, \boldsymbol{x}) \in \mathbb{C}^N$ and the measured impedance at the given frequencies $\boldsymbol{y} \in \mathbb{C}^N$ ($\boldsymbol{e} := \boldsymbol{Z} - \boldsymbol{y} = (\Re\{\boldsymbol{Z}\} - \Re\{\boldsymbol{y}\}) + j\,(\Im\{\boldsymbol{Z}\} - \Im\{\boldsymbol{y}\}) = (\boldsymbol{Z}_\Re - \boldsymbol{y}_\Re) + j\,(\boldsymbol{Z}_\Im - \boldsymbol{y}_\Im) = \boldsymbol{e}_\Re + j\boldsymbol{e}_\Im$). The equivalent impedance model is function of the specific frequency $f_k = \omega_k/2\pi$ at which it is calculated and of the values (all gathered in the vector of unknowns $\boldsymbol{x}$) of the circuit components which make up the equivalent model. Thus, the minimization of the normalized mean squared error can be written as

$$\min_{\boldsymbol{x}} \left[\boldsymbol{e}_\Re^T \boldsymbol{A}\hat{\boldsymbol{W}}\boldsymbol{A}\boldsymbol{e}_\Re + \boldsymbol{e}_\Im^T \boldsymbol{B}\tilde{\boldsymbol{W}}\boldsymbol{B}\boldsymbol{e}_\Im \right]^{\frac{1}{2}} \tag{5}$$

where $\hat{\boldsymbol{W}} = \mathrm{diag}(\hat{w}_1, \ldots, \hat{w}_N)$ and $\tilde{\boldsymbol{W}} = \mathrm{diag}(\tilde{w}_1, \ldots, \tilde{w}_N)$ are two weight matrices that can be suitably set to give more relevance to the real or imaginary part of the equivalent impedance Z and, possibly, to each single sample separately, and $\boldsymbol{A} = \mathrm{diag}(1/\Re\{y_1\}, \ldots, 1/\Re\{y_N\})$ and $\boldsymbol{B} = \mathrm{diag}(1/\Im\{y_1\}, \ldots, 1/\Im\{y_N\})$ are the two diagonal matrices used for the normalization.

If the model to be fitted is the one represented in Figure 1, then the vector of unknowns is $\boldsymbol{x} = [C_\mathrm{b}\ R_0\ R_\mathrm{f}\ C_\mathrm{f}\ R_\mathrm{s}\ C_\mathrm{s}]^T$ and the equivalent impedance $Z\,(\omega, \boldsymbol{x})$ is $R_0 + 1/j\omega C_\mathrm{b} + R_\mathrm{f}/\,(1 + j\omega R_\mathrm{f} C_\mathrm{f}) + R_\mathrm{s}/\,(1 + j\omega R_\mathrm{s} C_\mathrm{s})$. The problem represented in (5) is nonlinear.

The cell used for these tests is the Polymer Lithium-ion battery 8773160K manufactured by General Electronics Battery Co., Ltd. The characteristic data of cell are reported in Table. I.

Table I
Main data of the cell.

Item	Specifications
rated capacity	C5 =10 Ah
rated voltage	3.7 V
charge cut-off voltage	4.2 V
discharge cut-off voltage	2.75 V

The instrumentation used for the EIS procedure is a 100-A booster (VMP3B-100) connected to a potentiostat (SP-150), (both from Biologic Science Instruments), controlled by a PC via USB connection with EC-LAB software.

The measurement tests have been carried out at different OCVs. Starting from charge cut-off voltage (which, after a rest time interval, corresponds to a fully charged cell), the small-signal ac current is imposed to the cell in order to measure the impedance at the different frequencies. Then, an energy corresponding to 10% of the nominal energy is drawn from the cell and, before starting a new measurement campaign the cell is left idle for the rest time period. The procedure ends when the last measurement campaign is close to the nominal voltage. For this experiment the rest time interval has been set to 10 min. The complete voltage profile of the cell during the test is reported in Figure 2.

In the plot, the high frequency oscillations induced by the EIS procedure at the end of the rest time interval are evident. It can be easily seen that 11 measurements of the impedance have been carried out. It is worth noting

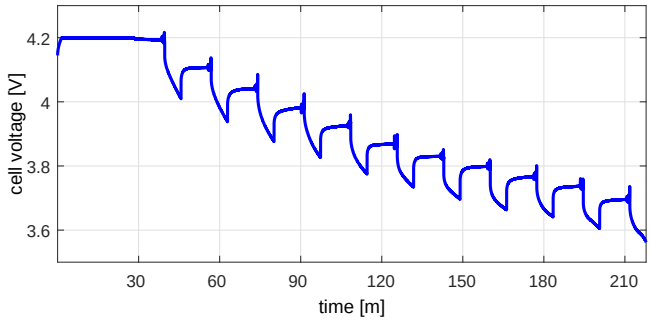

Figure 2. EIS procedure. Cell voltage profile during the procedure

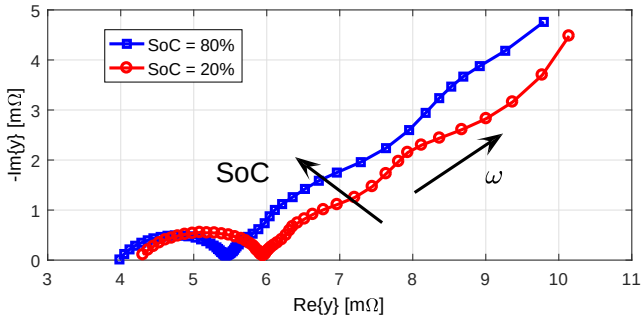

Figure 3. EIS procedure. Examples of the output of the EIS procedure for two different starting OCVs corresponding to SOC = 80% (blue square marker line) and SOC = 20% (red circle marker line), respectively.

that each measurement campaign can be identified by the starting SOC, rather than by the starting OCV (the two notions being practically the same). Two of these eleven curves are reported in Figure 3. In particular, the curves are those obtained during the third and the ninth iteration of the EIS procedure. They correspond to the impedance measured for SOC $= 80\%$ ($V_{\rm oc} = 4.041$ V) and SOC $= 20\%$ ($V_{\rm oc} = 3.767$ V). The bottom left values of the curves are calculated for frequencies of 1.5 kHz approximately, while the upper right values are calculated for $f = 1$ mHz. The right end of the half circles are calculated for frequencies of 1 Hz, approximately.

The values obtained by applying the minimization described in (5) are reported in Table II. The fitting has been performed with $\hat{\boldsymbol{W}} = \tilde{\boldsymbol{W}} = \boldsymbol{I}_N$. In the last column of Table II the mean values of each parameter are reported. These mean values have been used for the comparison of the effects of the parameters estimation techniques on SOC estimation algorithms.

C. ARMAX *Model Identification*

The ARMAX method identifies the parameters of the Randles model (see Figure 1) using controlled charge and discharge test results, as illustrated in [8], [16], [17]. In particular, a discharge test has been performed: starting from a state of total charge, the battery has been fully discharged through a sequence of current steps. Each step is 1 C-rate high ($I_{\rm B} = 10$ A) and long enough to reduce the SOC by 2%. The steps are followed by a 30 min pause, during which the system rests. Globally the test lasts for almost 26 h. All measurements are collected with 1 s granularity.

The OCV, $V_{\rm oc}$, is assumed equal to the voltage value measured at the end of the resting period. In Figure 4 the circles show when the $V_{\rm oc}$ evaluation is performed in a discharge test.

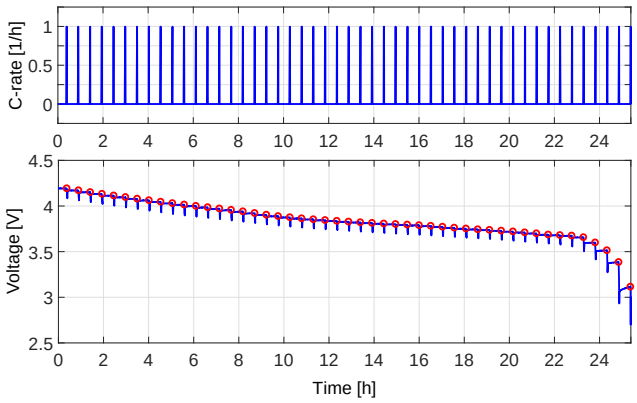

Figure 4. Current and voltage profiles during a discharge test.

During the tests, each $V_{\rm oc}$ value is collected together with the corresponding SOC. The 49 collected pairs of $(\text{SOC}, V_{\rm oc})$ values are registered and used to identify a fitting curve $V_{\rm oc}(\text{SOC})$. The best result has been obtained by adopting a truncated Fourier series fitting function of eighth order, depicted in Figure 5 together with the registered pairs $(\text{SOC}, V_{\rm oc})$.

Referring to model (1)–(4) proposed in Section II-A, (1) can be formulated in the Laplace domain as follows:

$$V_{\rm B}(s) = V_{\rm oc}(s) - R_0 I_{\rm B}(s) - G_m(s) I_{\rm B}(s), \qquad (6)$$

$$G_m(s) = \frac{R_{\rm s}}{1 + sR_{\rm s}C_{\rm s}} + \frac{R_{\rm f}}{1 + sR_{\rm f}C_{\rm f}}. \qquad (7)$$

The model parameters are identified as follows:

Table II
VALUES OF THE PARAMETERS OF THE EQUIVALENT IMPEDANCE OBTAINED THROUGH EIS PROCEDURE AND THE OPTIMIZATION IN (5).

	EIS 1	EIS 2	EIS 3	EIS 4	EIS 5	EIS 6	EIS 7	EIS 8	EIS 9	EIS 10	EIS 11	MEAN VALUES
$C_{\rm b}$ [F]	36000		38469	36000			39995	39996	36000	36003	36000	36951
R_0 [Ω]	0.0041	0.0041	0.0040	0.0040	0.0041	0.0041	0.0042	0.0044	0.0043	0.0043	0.0041	0.0042
$R_{\rm f}$ [Ω]	0.0034	0.0043	0.0044	0.0047	0.0039	0.0040	0.0036	0.0037	0.0042	0.0033	0.0043	0.0040
$C_{\rm f}$ [F]	9995	9990	7109	9988	9993	9992	6093	5448	9991	7081	9991	8697
$R_{\rm s}$ [Ω]	0.0016	0.0015	0.0014	0.0015	0.0014	0.0016	0.0016	0.0016	0.0016	0.0016	0.0016	0.0015
$C_{\rm s}$ [F]	0.6387	0.4493	0.6826	0.7125	1.5171	0.7344	0.7394	0.7976	0.8463	0.9011	0.9967	0.8196

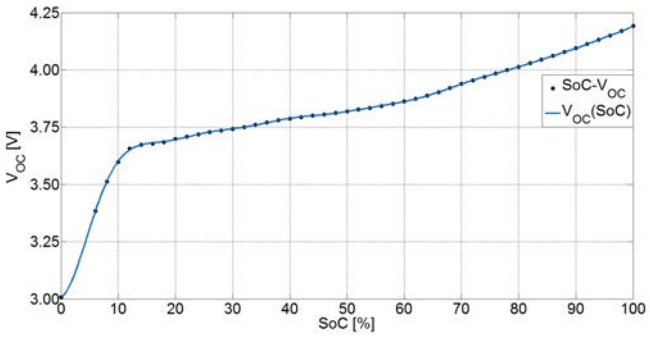

Figure 5. SOC-OCV map truncated Fourier series fitting curve. Black dots are the registered pairs $(\text{SOC}, V_{\text{oc}})$.

- C_b: excluding the temperature effects, the whole-charge capacity is equal to 3600×(Nominal Capacity)[Ah]. The resultant capacity is therefore C_{b} = 36000 F.
- R_0: the internal resistance is calculated as the ratio between the instantaneous voltage variation and the amplitude of the k-th current step as shown in Figure 6:

$$R_{0,k} = \frac{v_{\min,k} - v_{\max,k}}{i_{\min,k} - i_{\max,k}}. \tag{8}$$

The final value of R_0 is the mean value of whole set of the computed internal resistances $R_{0,k}$.

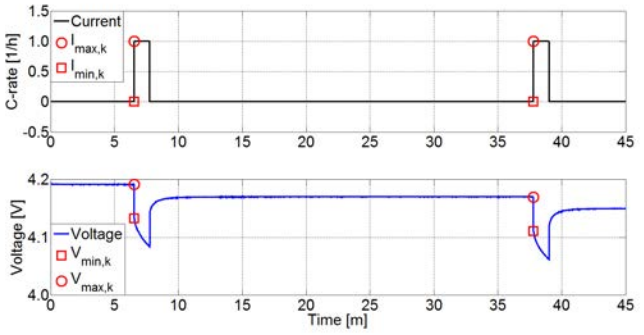

Figure 6. $R_{0,k}$ evaluation example.

- RC Network: relationship (6) can be rewritten as

$$V_{\text{oc}} - V_{\text{B}} - R_0 I_{\text{B}} = G_m I_{\text{B}} =: V_{\text{eq}}, \tag{9}$$

where, assuming $dI_{\text{B}}/dt = 0$ in the sampling period T_s = 1 s, time-discretization provides, using Z-transform:

$$\begin{aligned} V_{\text{eq}}(z) &= \left(\frac{R_{\text{f}}\left(1 - \exp(-T_s/T_{\text{pf}})\right) z^{-1}}{1 - \exp(-T_s/T_{\text{pf}}) z^{-1}} \right. \\ &\quad \left. + \frac{R_{\text{s}}\left(1 - \exp(-T_s/T_{\text{ps}})\right) z^{-1}}{1 - \exp(-T_s/T_{\text{ps}}) z^{-1}} \right) I_{\text{B}}(z) \\ &= \left(\frac{z^{-1}(b_1 + b_2 z^{-1})}{1 + a_1 z^{-1} + a_2 z^{-2}} \right) I_{\text{B}}(z) \end{aligned} \tag{10}$$

where, T_{ps}, T_{pf} are the time constants of the two RC sub-networks. Coefficients a_1, a_2, b_1, b_2 were identified by the ARMAX identification method [19]. The values were then used to define the parameters in Table II.

Table II
RC NETWORK PARAMETERS

PARAMETER	VALUE	PARAMETER	VALUE
R_0	6.1 mΩ	R_{f}	2.9 mΩ
C_{b}	36000 F	R_{s}	3.7 mΩ
T_{pf}	22.5 s	C_{f}	7745 F
T_{ps}	345.9 s	C_{s}	93472 F

III. THE SOC ESTIMATION ALGORITHM

This section briefly recalls the SOC estimation algorithm used in Section IV to analyze the impact of the two battery characterization methods above proposed on the estimation accuracy. The adopted estimation procedure is an extended Kalman filter (EKF) based on the truncated Fourier series representation of the nonlinear SOC-OCV map. In [8], such an approach is proved to have the best performances within a set of other candidate Kalman-based estimation procedures.

In order to introduce the estimation technique, model (2)–(4) is firstly written in the standard continuous-time state space form

$$\dot{x} = \bar{A}x + \bar{B}u \tag{11}$$

$$y = h(x) \tag{12}$$

where x, u and y are the system state, control and output vector, respectively defined as

$$x = \begin{bmatrix} V_f \\ V_s \\ V_{\text{SOC}} \end{bmatrix}, \quad u = I_B, \quad y = V_B, \tag{13}$$

and where

$$\bar{A} = \begin{bmatrix} -\frac{1}{R_f C_f} & 0 & 0 \\ 0 & -\frac{1}{R_s C_s} & 0 \\ 0 & 0 & 0 \end{bmatrix}, \quad \bar{B} = \begin{bmatrix} \frac{1}{C_f} \\ \frac{1}{C_s} \\ -\frac{1}{C_b} \end{bmatrix}, \tag{14}$$

$$h(x) = V_{\text{oc}}(x_3) - x_1 - x_2 - R_0 u \tag{15}$$

System (11)–(12) is nonlinear because of the SOC-OCV map appearing in the output map (15). Therefore, nonlinear Kalman filtering approaches are required. As for any model based estimation algorithm, nonlinear filtering performances depend on the model accuracy. In [8] three possible representations of the SOC-OCV map are considered. The one resulted to offer the best estimation results in terms of root mean square error (RMSE) is the truncated Fourier series fitting curve, which has the following form (expressed as function of $V_{\text{SOC}} = x_3$):

$$\begin{aligned} V_{\text{oc}}^F(x_3) =& a_0 + \\ &+ \sum_{n=1}^{8} [a_n(\cos(nwx_3)) + b_n(\sin(nwx_3))]. \end{aligned} \tag{16}$$

After time-discretization, system (11)–(12) assumes the form

$$x_{k+1} = Ax_k + w_k, \tag{17}$$

$$y_k = h(x_k) + v_k, \tag{18}$$

where $x_k = x(T_s k)$, $y_k = y(T_s k)$ and $A = e^{\bar{A}T_s}$. Sequences w_k and v_k are supposed to be zero-mean, white,

Gaussian and mutually independent. They are added to the state and output equations in order to represent the model uncertainties and the measurement errors (see [8] for more details). System (17)–(18) is amenable to be processed by the standard EKF algorithm [20], which operates the linearization of the output map (15) at each filtering step. EKF returns the estimate the state vector x_k, whose third component corresponds to the estimate of the SoC voltage V_{OC} at the time step k.

IV. Experimental Performances Evaluation

In order to analyze the impact of the battery characterization methods proposed in Section II, the EKF SOC estimation algorithm described in Section III has been applied to real experimental data based on the different set of parameters identified for the test Polymer Lithium-ion battery, using EIS and ARMAX techniques.

In the following, the EKF that uses the parameters identified by the ARMAX procedure is indicated with ARMAX EKF. In the same way, EIS 1–11 EKFs and mean EIS EKF indicate the EKF based on the parameters computed through the 11 EIS procedures and their mean values, respectively.

The test battery has been driven with three load current paths used as benchmark for electrical vehicles: New European Drive Cycle (NEDC) [21], which moves the SOC within the interval 80–63%; EPA Federal Test Procedure 72 (FTP-72) [22], which moves the SOC between 80–74%; and EPA Federal Highway Fuel Economy Test Procedure (HWFET) [23], which drives the SOC within the interval 83–52%. Each current path consists of a set of sub-profiles of 4–8 minutes, separated by pause intervals lasting from 1 to 2 hours.

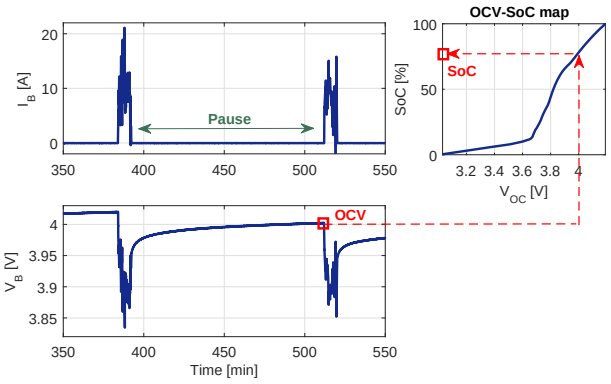

Figure 7. Sketch of the real SoC computation procedure.

As shown in Figure 7, during pauses, SOC does not change, whereas the measured terminal voltage V_B converges to the corresponding OCV. Therefore, a set of OCV values is collected for each current path by registering the terminal voltages V_B at the end of the pause intervals. The real SOC levels reached at the beginning of pauses are then post-computed from the collected OCVs by inverting the SOC-OCV map. The inverse map is obtained with high accuracy by employing the *spline smoothing fitting technique* over the same 49 pairs (SOC, V_{oc}) used to identify the direct SOC-OCV maps in Section II-C.

Figure 8 shows the absolute values of the SOC estimation errors, defined as the difference between the filters SOC

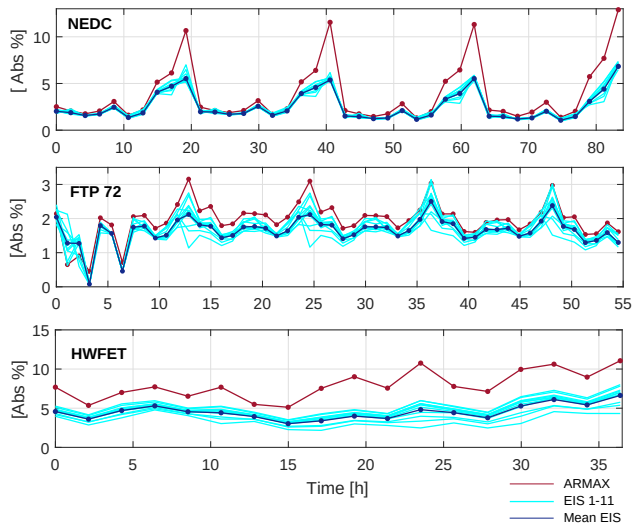

Figure 8. Experimental results: absolute values of the SOC estimation errors in correspondence of the *post-computed* real SOC values.

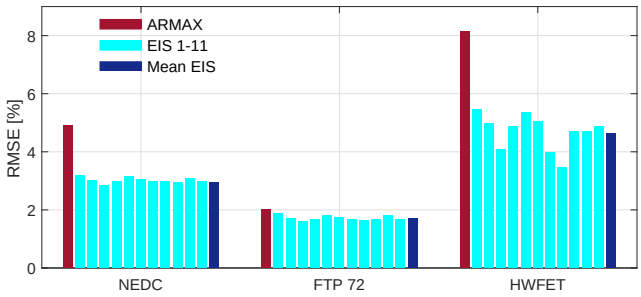

Figure 9. Experimental results: RMSEs.

estimates at the beginning of pauses and the *post-computed* real SOC values, returned by the ARMAX EKF (red line), by the EIS 1–11 EKFs (light blue lines), and by the mean EIS EKF (dark blue line). For all the three datasets, EIS EKF clearly over-performs the ARMAX EKF. This is particularly highlighted with the NEDC and HWFET current paths. Figure 9 shows the corresponding root mean square errors (RMSE), computed over the SOC estimation errors. In the cases of NEDC and HWFET current paths, the estimation performances result to be significantly sensitive to the values of the identified parameters. In these cases, the EIS 1–11 EKFs significantly improve the estimation accuracy of the ARMAX EKF. In particular the RMSE is reduced of about 2% in the NEDC case, and of about 2.5% in the HWFET case. There are no significant differences in the FTP-72 case, in which the overall SOC variation is less relevant. The results obtained by the EIS 1–11 EKFs are generally comparable each others, whereas the mean EIS EKF effectively returns average performances.

V. Conclusion

The work presented in this paper has focused on determining the effect of different battery equivalent model identification on SOC estimation. A Polymer Lithium-Ion cell has been characterized using two different approaches, namely EIS and ARMAX. The former follows a frequency-domain approach, and the latter a time-domain procedure.

Three power profiles (derived from driving test cycles) have been applied to the cell and the two dynamical models have been used to estimate the SOC. The analysis of the RMSEs shows that the estimation accuracy strongly depends on the precision of the estimated model parameters. In this terms, the EIS-based procedure has resulted to be more accurate with respect the ARMAX-based one. In conclusion, the EIS technique can be considered a suitable model identification method for developing high accuracy battery SOC estimators.

REFERENCES

[1] F. Baccino, S. Grillo, M. Marinelli, S. Massucco, and F. Silvestro, "Power and energy control strategies for a vanadium redox flow battery and wind farm combined system," in *IEEE PES International Conference and Exhibition on Innovative Smart Grid Technologies (ISGT Europe)*, Dec. 2011.

[2] F. Baccino, M. Marinelli, P. Nogard, and F. Silvestro, "Experimental testing procedures and dynamic model validation for vanadium redox flow battery storage system," *J. Power Sources*, vol. 254, pp. 277–286, 2014.

[3] F. Conte, S. Massucco, M. Saviozzi, and F. Silvestro, "A Stochastic Optimization Method for Planning and Real-Time Control of Integrated PV-Storage Systems: Design and Experimental Validation," *IEEE Trans. Sust. Energy*, 2017, doi: 10.1109/TSTE.2017.2775339.

[4] F. Adinolfi, F. Conte, F. D'Agostino, S. Massucco, M. Saviozzi, and F. Silvestro, "Mixed-integer algorithm for optimal dispatch of integrated PV-storage systems," in *17th IEEE International Conference on Environment and Electrical Engineering and 2017 1st IEEE Industrial and Commercial Power Systems Europe*, 2017.

[5] L. Canals, A. S. Gonzalez, B. Amante, and J. Llorca, "PHEV battery ageing study using voltage recovery and internal resistance from On-board data," *IEEE Trans. Veh. Technol.*, vol. 65, no. 6, pp. 4209–4216, Jun. 2016.

[6] S. Mohan, Y. Kim, and A. G. Stefanopoulou, "Estimating the Power Capability of Li-ion Batteries Using Informationally Partitioned Estimators," *IEEE Trans. Control Syst. Technol.*, vol. 24, no. 5, pp. 1643–1654, Sep. 2016.

[7] S. Barcellona, S. Grillo, and L. Piegari, "A simple battery model for ev range prediction: Theory and experimental validation," in *IEEE ESARS ITEC*, 2016.

[8] F. Adinolfi, F. Conte, S. Massucco, M. Saviozzi, F. Silvestro, and S. Grillo, "Performance Evaluation of Algorithms for the State of Charge Estimation of Storage Devices in Microgrid Operation," in *2016 Power Systems Computation Conference (PSCC)*, Jun. 2016.

[9] M. Cacciato, G. Nobile, G. Scarcella, and G. Scelba, "Real-time model-based estimation of SOC and SOH for energy storage systems," *IEEE Trans. Power Electron.*, vol. 32, no. 1, pp. 794–803, Jan. 2017.

[10] S. Piller, M. Perrin, and A. Jossen, "Methods for state-of-charge determination and their applications," *J. Power Sources*, vol. 96, no. 1, pp. 113–120, Jun. 2001.

[11] D. V. Do, C. Forgez, K. E. K. Benkara, and G. Friedrich, "Impedance observer for a li-ion battery using kalman filter," *IEEE Trans. Veh. Technol.*, vol. 58, no. 8, pp. 3930–3937, Oct. 2009.

[12] M. Li, "Li-ion dynamics and state of charge estimation," *Renew. Energy*, vol. 100, pp. 44–52, Jan. 2017.

[13] F. Codecà, S. M. Savaresi, and V. Manzoni, "The mix estimation algorithm for battery state-of-charge estimator-analysis of the sensitivity to measurement errors." in *48th IEEE Conference on Decision and Control*, 2009, pp. 8083–8088.

[14] G. Pérez, M. Garmendia, J. F. Reynaud, J. Crego, and U. Viscarret, "Enhanced closed loop State of Charge estimator for lithium-ion batteries based on Extended Kalman Filter," *App. Energy*, vol. 155, pp. 834–845, 2015.

[15] M. Chen and G. Rincon-Mora, "Accurate electrical battery model capable of predicting runtime and i-v performance," *IEEE Trans. Energy Convers.*, vol. 21, no. 2, pp. 504–511, Jun. 2006.

[16] P. Spagnol, S. Rossi, and S. Savaresi, "Kalman Filter SoC estimation for Li-Ion batteries," in *IEEE International Conference on Control Applications (CCA)*, Sep. 2011, pp. 587–592.

[17] M. Gholizadeh and F. Salmasi, "Estimation of State of Charge, Unknown Nonlinearities, and State of Health of a Lithium-Ion Battery Based on a Comprehensive Unobservable Model," *IEEE Trans. Ind. Electron.*, vol. 61, no. 3, pp. 1335–1344, Mar. 2014.

[18] P. Agarwal, M. E. Orazem, and L. H. Garcia-Rubio, "Measurement Models for Electrochemical Impedance Spectroscopy I. Demonstration of Applicability," *J. Electrochem. Soc.*, vol. 139, no. 7, pp. 1917–1927, Jul. 1992.

[19] M. Verhaegen and V. Verdult, *Filtering and System Identification: A Least Squares Approach*. Cambridge University Press, 2007.

[20] B. D. O. Anderson and J. B. Moore, *Optimal filtering*. Prentice-Hall, 1979.

[21] Council of European Union, "Agreement Concerning the Adoption of Uniform Technical Prescriptions for Wheeled Vehicles, ..." Apr. 2013, E/ECE/324/Rev.2/Add.100/Rev.3–E/ECE/TRANS/505/Rev.2/Add.100/Rev.3 [Online]. Available: http://www.unece.org/trans/main/wp29/wp29regs101-120.html.

[22] United States Environmental Protection Agency, "Control of Emissions From New And In-Use Highway Vehicles and Engines," Jul. 2006, Title 40 CFR Chapter I Subchapter C Part 86 , Appendix I [Online]. Available: http://www.gpo.gov.

[23] ——, "Fuel Economy of Motor Vehicles," Jul. 2003, Title 40 CFR Chapter I Subchapter Q Part 600, Appendix I [Online]. Available: http://www.gpo.gov.